High Hydrides of Scandium under Pressure: Potential Superconductors

Xiaoqiu Ye,[†,‡] Niloofar Zarifi,[‖] Eva Zurek,*[,‖] Roald Hoffmann,*[,‡] and N. W. Ashcroft[§]

[†]China Academy of Engineering Physics, Mianyang, Sichuan 621900, China

[‡]Department of Chemistry and Chemical Biology and [§]Laboratory of Atomic and Solid Physics, Cornell University, Ithaca, New York 14853, United States

[‖]Department of Chemistry, State University of New York at Buffalo, Buffalo, New York 14260-3000, United States

Ⓢ Supporting Information

ABSTRACT: In a systematic investigation of scandium hydrides with high hydrogen content we predict seven phases of scandium hydrides (ScH_4, ScH_6, ScH_7, ScH_8, ScH_9, ScH_{10}, and ScH_{12}), which are stable above 150 GPa. Zero point energies are essential in determining the phases and pressure ranges within which they are stable. The interconversion of the various hydrides is intriguing; in one case there is a "return" to a lower hydrogen content hydride with increasing pressure. We argue that these hydrides may be synthesized by compressing mixtures of ScH_3 and H_2 above 150 GPa. New H bonding motifs are uncovered, including "H_5" pentagons or "H_8" octagons in ScH_9, ScH_{10}, and ScH_{12}. High T_cs are predicted for ScH_6, ScH_7, ScH_9, ScH_{10}, and ScH_{12}, with superconducting transition temperatures (T_cs) of 120−169 K above 250 GPa, as estimated by the Allen−Dynes modified McMillan equation.

I4₁md ScH_9 at 300 GPa

T_c:163 K

Immm ScH_{12} at 350 GPa

T_c: 141 K
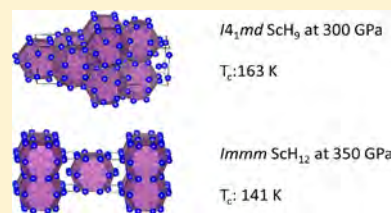
1. INTRODUCTION

Hydrogen-rich compounds have been recognized as a parallel route to the metallization of hydrogen itself, as in these metal−hydrogen alloys the combination of chemical precompression or doping of the light elements by the metal host coupled with experimentally applied pressures could create hydrogen densities in the range where metallization can occur.[1,2] The result would then be a very hydrogen-rich binary metal, with the enticing possibility that it may exhibit a high superconducting transition temperature (T_c) reflecting the dominance of hydrogen itself.

The quest for metallic and superconducting hydrides has been pursued by several theoretical groups—we mention here investigations of alkali and alkaline earth hydrides,[3−7] group 14 hydrides,[8] tungsten hydrides,[9] niobium hydrides,[10] and yttrium hydrides,[11] some of these carried out by us. Indeed, very high T_cs have been calculated for a number of metal hydrides, such as LiH_6 (82 K at 300 GPa),[3,12] MgH_6 (271 K at 300 GPa),[13] CaH_6 (235 K at 150 GPa),[4] YH_6 (264 K at 120 GPa),[11] YH_{10} (326 K at 250 GPa and 303 K at 400 GPa),[14] and LaH_{10} (286 K at 210 GPa).[14] So far, none of these have been experimentally realized, but the prospect has nevertheless been encouraged (if not fueled) by the recent discovery of remarkably high temperature superconductivity, with T_c up to 203 K, in compressed H_2S at ∼200 GPa;[15] theoretical and experimental investigations appear to have converged on the superconducting phase as being H_3S.[16,17] Recently, a T_c of ∼100 K at high pressures has been measured for compressed phosphine,[18] and theoretical studies predicting the phases that may contribute to the superconductivity have been performed.[19−21]

We add to the aforementioned hydride systems with moderate to high T_cs with the present work on high hydrides of scandium. Interest in scandium and its hydrides derives as well from their potential for hydrogen storage and from their intriguing and complex structural, electronic, and vibrational properties.[22] In our previous work,[23] we investigated the fascinating phase separation phenomena of the low scandium hydrides and found that ScH_3 is stable over a very wide pressure range of 0−400 GPa. The consistency with experiment of the geometries we found for ScH, ScH_2, and ScH_3, and of the details of the disproportionation reaction of ScH_2, encourages us to examine the higher hydrides.

Sc is the lightest element, with the smallest ionic radius, among the transition metals. It may be easy to add small amounts of Sc to hydrogen. The propensity for superconductivity in a hydride of scandium is also encouraging: it lies in a region of the periodic table where theoretical calculations have predicted other hydrides with high T_cs may be stabilized under pressure (Mg,[13] Ca,[4] Sr,[24] Y,[14] and La[14]). Estimates for the T_c of the hydrides of scandium with $n \leq 3$ have been previously provided: ScH_2 (38 K at 30 GPa[25]) and ScH_3 (19 K at 18 GPa[26]).

Very recently, several theoretical studies of the structures of, and superconductivity in compressed scandium hydrides have been reported. The calculations of Abe[27] considered ScH_4, ScH_5, and ScH_6 stoichiometries and predicted that the following phases will be stable: *I4/mmm* ScH_4 above ∼160 GPa, *P6₃/mmc* ScH_6 from 135 to 265 GPa, and *Im-3m* ScH_6

above 265 GPa. Qian and co-workers also found these same stable phases, though in slightly different pressure ranges.[28] This group also considered ScH_7 and ScH_8 stoichiometries and predicted a stable ScH_8 phase with $Immm$ symmetry above 300 GPa. Finally, in addition to $I4/mmm$ ScH_4, $P6_3/mmc$ ScH_6, and Im-$3m$ ScH_6, recent calculations by Peng et al.[29] further predicted that the $P6_3/mmc$ ScH_9, $Cmcm$ ScH_{10}, and $C2/c$ ScH_{12} phases become stable above 300 GPa, and the T_c of ScH_9 at 400 GPa was estimated to approach 200 K.

In work that began while these studies were carried out, we analyze hypothetical ScH_n ($n = 4-12$) stoichiometries, all studied over a range of pressures up to 400 GPa, with relative compressions reaching $V_0/V \sim 4$ (V_0 is the volume of the most stable phase at 1 atm, and V is the volume of the most stable phase at a given pressure). We examine in detail the optimum static structures of the various hydrides as a function of pressure, as well as their dynamical stability, electronic structures and superconducting properties. We find that most of the hydrides of scandium can become superconducting, with a relatively high calculated T_c (as the published studies cited also do). Some intriguing hydrogenic structural motifs emerge in the structures of these hydrides. Many of the structures we find correspond to those recently predicted by Abe, Qian, Peng, and their co-workers. However, the $I4_1md$ ScH_9 and $Immm$ ScH_{12} phases predicted in our work have somewhat lower enthalpies than those found by Peng et al.[29] Moreover, the $Cmcm$ ScH_6, and the $Cmcm$ ScH_7 phases have not been found in previous studies. And, we believe that we provide the most comprehensive analysis carried out to date of the structures of these unique phases as well as the enthalpic interconversions between them.

2. COMPUTATIONAL METHODS

We searched extensively for ScH_n ($n = 4-12$) ground-state structures using the particle swarm optimization methodology implemented in the CALYPSO code.[30] This method has been applied successfully to a wide range of crystalline systems ranging from elemental solids to binary and ternary compounds.[30] Our structure searches with system sizes containing up to 6 formula units (fu) per simulation cell were performed at pressures of 0−400 GPa. Each generation contained 30−40 structures (the larger the system, the larger the number of structures). We usually followed 30−50 generations (depending on the size of the system) to find the lowest enthalpy structure. We also checked the results by alternative generation of structures using evolutionary algorithms (EAs) as implemented in XTALOPT.[31] XTALOPT uses a population-based pool, instead of a generation-based one, so that a new "offspring" is created as soon as a single structure has finished optimizing. In each EA run multiple formula units can be considered simultaneously: here we employed 2−8 formula units in the searches carried out for ScH_4 at 120 and 250 GPa, ScH_5 at 300 GPa, ScH_6 at 250 GPa, and ScH_{10} at 250 GPa. In addition, we carried out geometry optimizations of the ScH_9 and ScH_{12} phases found by Peng et al.[29] and the scandium analogues of the $(Y/La)H_{10}$ structures in the Fm-$3m$ space group, as well as the $(Y/La)H_9$, $(Y/La)H_{12}$ and the YH_8 structures in the $C2/c$ space group,[14] the UH_7 and UH_9 structures in the $P6_3/mmc$ space group,[32] and the UH_8 structure in the Fm-$3m$ space group,[32] which were predicted to be particularly stable.[14,32] As shown in Figures S48−S51 of the Supporting Information (SI), the phases predicted herein all had lower enthalpies up to at least 400 GPa. Moreover, only

the $C2/c$ ScH_{12} analogue was computed to be dynamically stable; the other phases derived from Y/La/U hydrides were not.

The underlying structural relaxations were carried out using density functional theory and the Perdew−Burke−Ernzerhof exchange-correlation functional[33] as implemented in the VASP code.[34] The projector-augmented wave method[35] was adopted, with $1s^1$ (cutoff radius of $1.1a_0$; we also tried some of our calculations with a smaller cutoff radius of $0.8a_0$, which did not change our major conclusions) and $3s^2 3p^6 3d^1 4s^2$ (cutoff radius of $2.5a_0$) treated as valence electrons for H and Sc, respectively. An energy cutoff of 800 eV and appropriate Monkhorst−Pack[36] k-meshes were chosen to ensure that enthalpy calculations were well-converged to better than 1 meV/atom. Phonon calculations were carried out using VASP in conjunction with the PHONOPY code.[37] To check the influence of magnetic/spin−orbit factors on the stability, both spin-polarized and spin−orbit coupling (SOC) were included in structural optimizations of ScH_n ($n = 3, 4, 6$). Here we considered three possibilities for the magnetic states: nonferromagnetic (NM), ferromagnetic (FM), and antiferromagnetic (AFM). In the AFM calculations, we used the collinear $1 - k$ structure where the atomic spin moment is along the [001] direction.

The superconducting critical temperature, T_c, was calculated using the Quantum Espresso (QE)[38] program package to obtain the dynamical matrix and the electron−phonon coupling (EPC) parameters. In the QE calculations, the H pseudopotential, obtained from the QE pseudopotential library, was generated by the method of Trouiller−Martins[39] with $1s^1$ valence configurations, and for Sc we employed an ultrasoft pseudopotential from the GBRV library,[40,41] which consisted of the $3s^2 3p^6 4s^2 3d^1$ valence configurations. Both pseudopotentials include the PBE generalized gradient approximation. Plane-wave basis set cutoff energies were set to 80 Ry for all systems. The Brillouin-zone sampling scheme of Methfessel−Paxton[42] using a smearing of 0.03 Ry and dense k-point grids was used for all calculations carried out on the ScH_n phases. Density functional perturbation theory[43] as implemented in QE was employed for the phonon calculations. The EPC parameter, λ, was calculated using a set of Gaussian broadenings in steps of 0.005 Ry from 0 to 0.300 Ry. The broadenings for which λ was converged to within 0.05 were between 0.015 and 0.055 Ry for all structures. T_c has been estimated using the Allen−Dynes modified McMillan equation[44]

$$T_c = \frac{\omega_{\log}}{1.2} \exp\left[-\frac{1.04(1 + \lambda)}{\lambda - \mu^*(1 + 0.62\lambda)}\right]$$

where $\omega_{\log}$ is the logarithmic average frequency and μ^*, the Coulomb pseudopotential, was taken to be 0.1. In addition, T_c was calculated by numerically solving the Eliashberg equations based on the spectral function, $\alpha^2 F(\omega)$, obtained with QE and using $\mu^* = 0.1$.[45]

3. RESULTS AND DISCUSSION

3.1. Stabilities for Different Stoichiometries under Pressure. The enthalpies of candidate structures of ScH_n ($n = 4-12$) found by us are plotted in a typical convex hull diagram, indicating compositions relative to ScH_3 + solid H_2 at selected pressures, in Figure 1. This choice of the reference system simply comes from our previous findings that ScH_3 is quite stable to decomposition into the elemental phases under pressure and assumes Fm-$3m$ symmetry up to about 360 GPa

(a) Without ZPE

(b) With ZPE
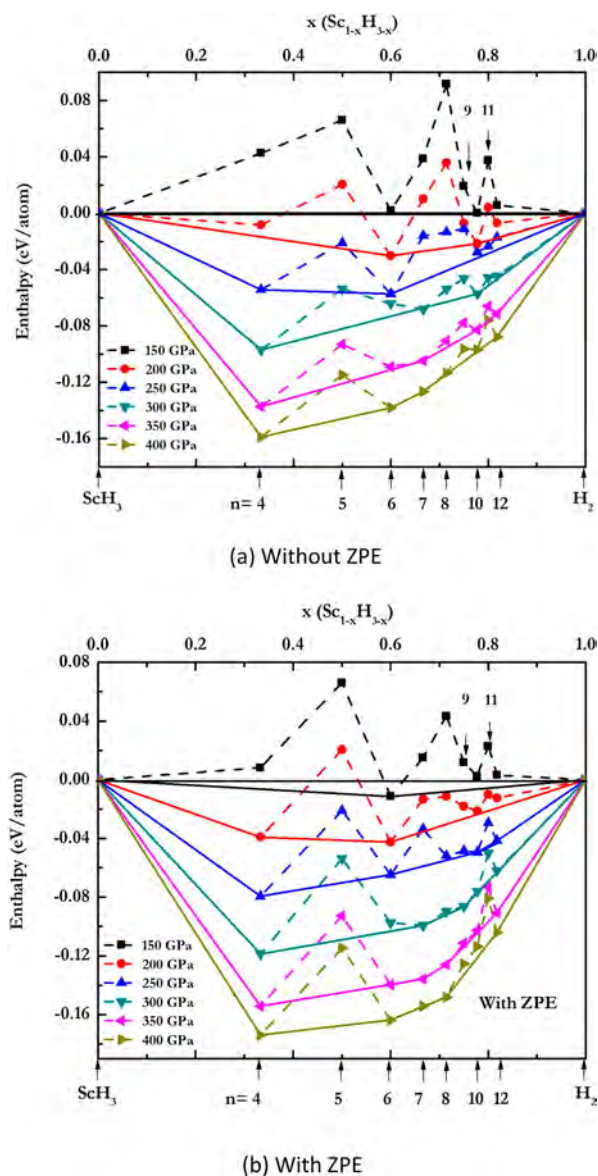
Figure 1. Enthalpy per atom of $Sc_{1-x}H_{3-x}$ as a function of x. The enthalpy is given relative to that of the system consisting of ScH_3[23] and H_2[46] phases. The zero-point energy (ZPE) is (a) omitted (static) and (b) included (dynamic) in the calculations. The stoichiometric index n (in ScH_n) is indicated at the bottom. The compositions on the solid line are stable at the corresponding pressure, while those on dashed lines are unstable with respect to decomposition or disproportionation into other hydrides and potentially molecular hydrogen (but they may be dynamically stable).

and $P6_3/mmc$ symmetry above 360 GPa.[23] The convex hull diagram with respect to Sc + solid H_2 and the detailed enthalpy curves of each hydride are provided in the Supporting Information.

In agreement with previous findings,[27−29] $I4/mmm$ ScH_4, $P6_3/mmc$ ScH_6, $Im-3m$ ScH_6, and $Cmcm$ ScH_{10} are predicted to be stable in our work, each in a particular pressure range between 150 and 400 GPa. ScH_{12} also emerges as being stable. However, our preferred ScH_{12} structure assumes $Immm$ symmetry, and its enthalpy is lower than the $C2/c$ ScH_{12} structure found previously.[29] Interestingly, a hitherto unobserved $Cmcm$ ($Z = 4$) ScH_7 structure is predicted to be stable

above 300 GPa while ScH_5, ScH_8, ScH_9, and ScH_{11} are not stable in the pressure range studied, as shown in Figure 1a.

In these hydrogen-rich structures the effects of the zero-point energy (ZPE) can be important in determining structural stability. Usually, compounds with a larger fraction of hydrogen atoms or a low crystal symmetry yield larger ZPEs. Moreover, the hydrogenic motifs present within a lattice influence its ZPE, and typically the ZPE increases with increasing pressure. A convex hull diagram where the ZPE effects are included is shown in Figure 1b. With the ZPE considered, ScH_8, and ScH_9 are also found on the convex hull together with the stable scandium hydrides discussed above. ScH_8 has $Immm$ symmetry as reported before[28] while ScH_9 has $I4_1md$ symmetry. The reported $P6_3/mmc$ ScH_9[29] phase has a higher enthalpy. Interestingly, we find that ScH_9 is stable in a narrow pressure range around 300 GPa, while ScH_8 is only stable above 320 GPa, as shown in Figure S35. ScH_7 with $Cmcm$ symmetry becomes stable above 280 GPa.

The influence of magnetic/spin−orbit effects on the stability of a few of the phases was investigated. We did not expect these factors to be important since Sc is not a heavy element, and charge is donated from its d-shell to the hydrogen atoms in these phases. As shown in the Figure S2, our expectations proved to be correct.

Figure 2 displays the pressure−composition phase diagram of the predicted stable hydrides of scandium. When the ZPE is
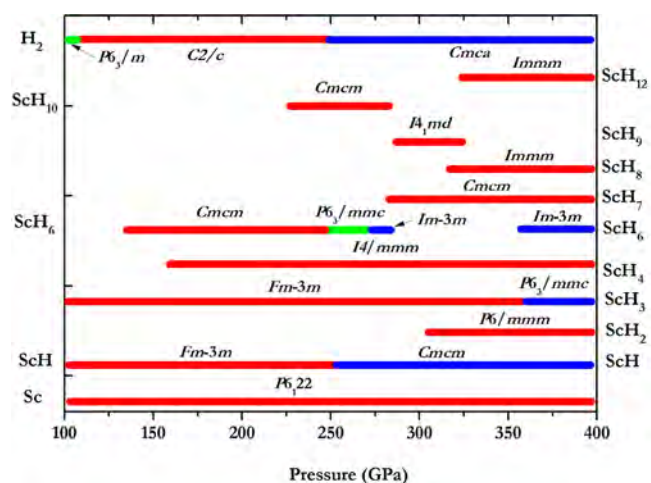
Figure 2. Predicted pressure−composition phase diagram of the Sc−H system, with ZPE included. For Sc, we used the $P6_122$ phase (Sc-V) to represent Sc-II, Sc-III, and S-IV in the pressure range from 100 to 400 GPa, since these phases of Sc are too complex to resolve either experimentally or theoretically.[47] The errors in the enthalpy from this assumption do not change our conclusions.[23]

included, the following phases are stable: $I4/mmm$ ScH_4 above 160 GPa, $Cmcm$ and then $P6_3/mmc$ ScH_6 from 135 to 275 GPa, $Im-3m$ ScH_6 between 275 and 285 GPa and then above 355 GPa, $Cmcm$ ScH_7 above 280 GPa, $Immm$ ScH_8 above 320 GPa, $I4_1md$ ScH_9 between 285 and 325 GPa, $Cmcm$ ScH_{10} between 220 and 285 GPa, and $Immm$ ScH_{12} above 325 GPa. As we can see, stable phases based on most stoichiometries can be found below 400 GPa, the only exception being ScH_5 and ScH_{11}. However, it may be that larger unit cells than those considered herein are required to find the most stable structures for these compositions.

Interestingly, we find that ScH_6 is unstable to decomposition into ScH_4 and ScH_7 at 300 GPa, as shown in Figures 1b and 2, and that at pressures near those in the earth's core ScH_{10} will decompose into ScH_9 and H_2. It seems that phase segregation reactions of these hydrides may be common under pressure. We will return to the intriguing interconversions between the various structures after presenting an initial discussion of the calculated structure types. As shown below, the geometries assumed by the scandium hydrides under pressure are complex, and many of them differ from those of the yttrium/lanthanum hydrides.[14,29]

3.2. Predicted ScH_n Structures. ScH_2 and ScH_3 are the experimentally known scandium hydrides. The structure search readily reproduced the observed structure of ScH_2 at 1 atm and of ScH_3 between 25 and 350 GPa, respectively, both based on fcc arrays of the transition metal ions. At 1 atm, ScH_2 adopts the $Fm\text{-}3m$ structure (CaF_2 type, $Z = 4$, Figure 3a). All hydrogens occupy the tetrahedral holes of the fcc lattice. The calculated Sc−H separations of 2.07 Å match the experimental crystallographic values at $P = 1$ atm.[48]
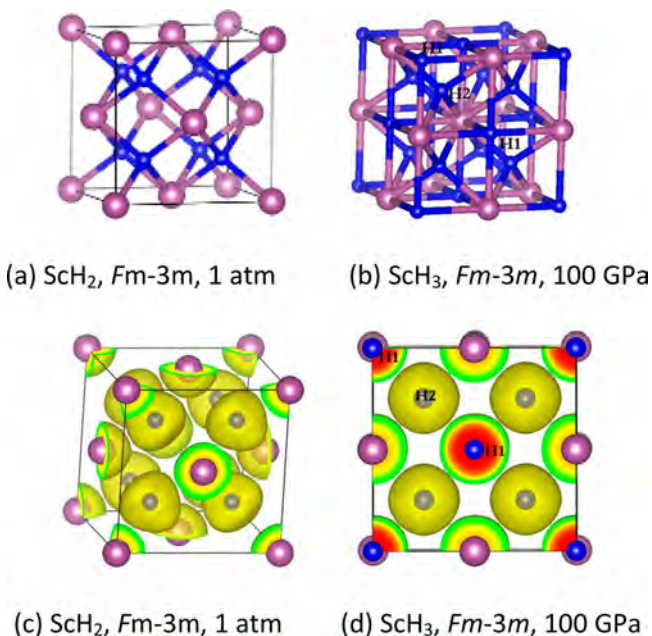
Figure 3. (a, b) Predicted ground-state static structures of ScH_2 and ScH_3. Large balls are Sc, and small balls are hydrogen. Lines are drawn for Sc−H separations shorter than 2.10 Å. (c, d) Three-dimensional electron localization functions (ELF) with an isosurface value of 0.5.

In ScH_3 the Sc atoms occupy fcc sites with two types of nonequivalent hydrogen atoms at the octahedral (H1) and tetrahedral (H2) sites, as shown in Figure 3b. The closest H−H separation is 2.40 Å at 1 atm in fcc-ScH_2 and 1.80 Å at 100 GPa in fcc-ScH_3; these distances and the plots of the electron localization function (ELF)[49] in Figures 3c and 3d clearly indicate no interaction between the H atoms.

As the pressure increases, seven more stoichiometries, ScH_4, ScH_6, ScH_7, ScH_8, ScH_9, ScH_{10}, and ScH_{12}, are found to become thermodynamically stable. Among the stable phases, $I4/mmm$ ScH_4, $P6_3/mmc$ ScH_6, $Im\text{-}3m$ ScH_6, $Immm$ ScH_8, and $Cmcm$ ScH_{10} have been reported before, while $Cmcm$ ScH_6, $Cmcm$ ScH_7, $I4_1md$ ScH_9, and $Immm$ ScH_{12} are for the first time predicted here. The ranges of stability are shown in Figure 2.

ScH_4 is a stable phase between 156 and 400 GPa, and it is the lowest point on the convex hull diagram of Figure 1b above 200 GPa. Details of the optimum calculated ScH_4 geometry and the enthalpy curves are given in the Supporting Information. This $I4/mmm$ phase has previously been reported for ScH_4[27−29] as well as in CaH_4[4] and SrH_4.[24,50]

Three phases, with the ScH_6 stoichiometries, were found to be stable in different pressure ranges. Their structures and ELF plots are provided in Figure 4. Interestingly, the $Cmcm$
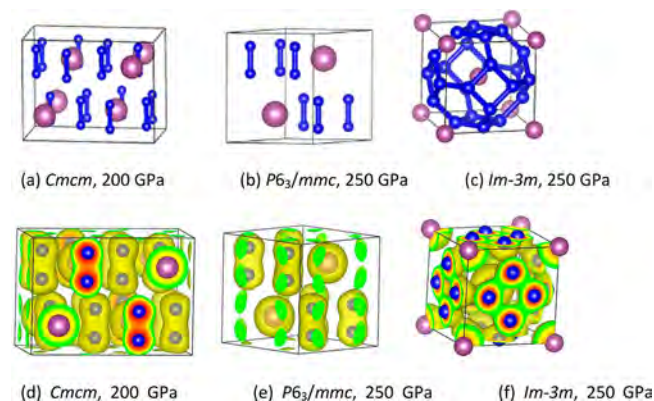
Figure 4. (a−c) Predicted ground-state static structures of ScH_6. Large balls are Sc, and small balls are hydrogen. The lines indicate H−H separations shorter than 1.20 Å. (d−f) Three-dimensional ELF with isosurface values of 0.5.

structure of ScH_6 ($Z = 4$) is calculated by us to be stable above 135 GPa, which is lower than the onset of stabilization of $I4/mmm$ ScH_4, as shown in the next section. The $Cmcm$ structure of ScH_6 contains an orthorhombic arrangement of Sc and six quasi-molecular "H_2" units (H−H separations of 1.00 Å at 250 GPa) around each Sc atom $(Sc_2(H_2)_6)$. The covalent interaction between H atoms is clearly visible from a plot of the electron localization function, prominent between the H atoms. We nevertheless put the molecular descriptor in quotes, as the H···H separation is substantially longer than that in H_2 itself at the same pressure, 0.76 Å.[46]

The evolution of the structures of ScH_6 with pressure is complex, as shown in Figure S11 and in the discussion to come. In our calculations, the $Cmcm$ structure of ScH_6 will turn into a $P6_3/mmc$ ($Z = 2$) structure above 200 GPa, with the small tolerance used in the automated symmetry assignment (CASTEP[51] with tolerance smaller than 0.01). And above 275 GPa, a sodalite-like structure ($Im\text{-}3m$, $Z = 2$) of ScH_6 emerges as being preferred, when ZPEs are taken into account. The shortest H−H separation in $Im\text{-}3m$ ScH_6 is 1.15 Å at 250 GPa. In this structure, H atoms form square "H_4" units on each face of a cage surrounding a Sc atom. The covalent interaction between H atoms is clearly visible in the ELF plot. This same sodalite structure is also found in YH_6 (110 GPa),[11] CaH_6 (150 GPa),[4] and MgH_6 (300 GPa).[13]

As we will see, this high-pressure structure of ScH_6 is not stable with respect to further hydrogenation. As the $Cmcm$ structure of ScH_6 continues to absorb hydrogen, it can transform to the $Cmcm$ structure of ScH_{10} ($Z = 4$, Figure 5a) above 220 GPa (see Figure S23). The nearest-neighbor H−H separation in $Cmcm$ ScH_{10} is 0.85 Å at 250 GPa. Interestingly, ScH_{10} is a layered structure where the Sc and H atoms are in one plane and the H atoms form unique "H_5" pentagons: one closed pentagon is edge-shared by two open pentagons. As
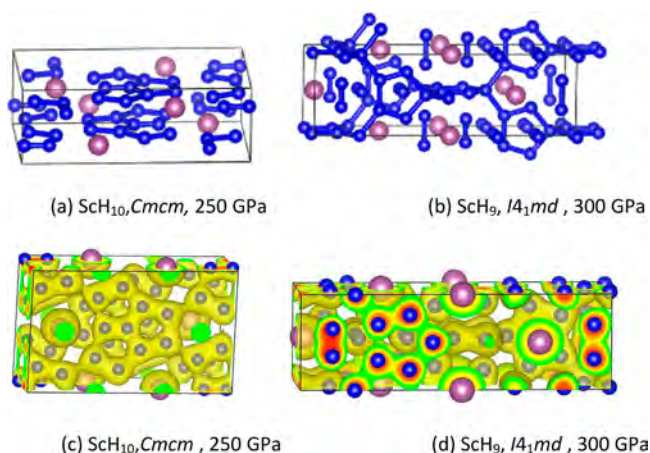
Figure 5. (a, b) Predicted ground-state static structures of ScH_{10} at 250 GPa and ScH_9 at 300 GPa. Large balls are Sc, and small balls are hydrogen. The lines indicate H−H separations shorter than 1.17 Å. (c, d) Three-dimensional ELF with isosurface values of 0.5.

Figure 2 indicates, the range of stability of ScH_{10} is limited. The *Cmcm* structure of ScH_{10} should decompose to the $I4_1md$ structure (tetragonal, $Z = 4$, Figure 5b) of ScH_9 and H_2 above 285 GPa. In $I4_1md$ ScH_9 at 300 GPa, the shortest H−H separation is 0.90 Å. One sees both molecular "H_2" and "H_5" pentagons in ScH_9. The interactions between neighboring hydrogens for both structures are seen clearly in the ELF plots (see Figures 5c and 5d).

Moving to still higher pressure, above 325 GPa, we calculate that ScH_9 should continue to absorb hydrogen and transform to an *Immm* structure (orthorhombic, $Z = 2$, Figure 6) of ScH_{12}. ScH_{12} is also a layered structure where the Sc and H atoms are in one plane, and H atoms form "H_5" pentagons. These "H_5" units are interlinked to form a 1D framework: six edges of each "H_8" octagon are connected by "H_5" pentagons, and the other two opposite edges are connected by another "H_8" octagon. Sc atoms lie at the edge of each substructure, in a
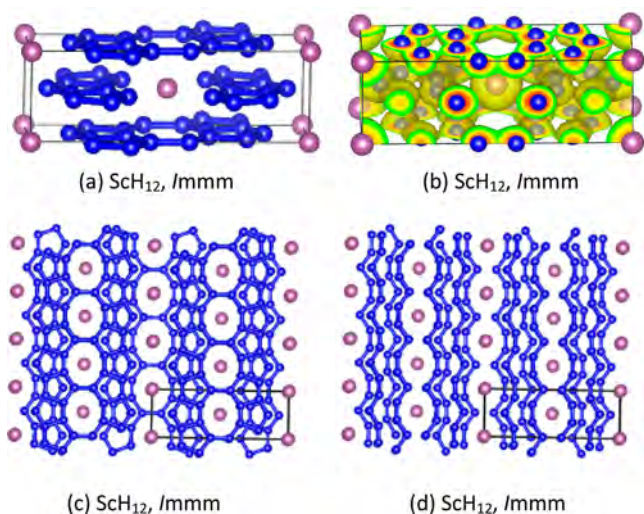
Figure 6. (a) Predicted ground-state static structures of ScH_{12} at 350 GPa. Large balls are Sc, and small balls are hydrogen. The lines indicate H−H separations shorter than 1.20 Å. (b) Three-dimensional ELF with isosurface value of 0.5. (c, d) Top view of the structure of ScH_{12}. The cutoff separation used to connect the hydrogen atoms is 1.20 Å in (a−c), while it is 1.05 Å in (d).

way enclathrated by the hydrogen framework. The shortest H−H separation is 0.91 Å in *Immm* ScH_{12} at 350 GPa. The hydrogen sublattice in this phase is very much interconnected; if we use 1.05 Å as the cutoff distance for plotting the H−H separation, we see one-dimensional ribbons in ScH_{12}.

It has been proposed that solid hydrogen adopts a layered structure (orthorhombic, *Cmca*, $Z = 12$) between 250 and 400 GPa, called phase IV.[46,52] The shortest H−H separation in this phase is 0.76 Å; the structure contains both graphene-like sheets and isolated H_2 units. It is very likely that the hydrogen atoms in the hydrogen-rich ScH_{12} form their own layered arrangements to keep to some extent the characteristics of solid hydrogen at similar pressures.

Two other phases that we found, ScH_7 and ScH_8, are stable above 280 and 320 GPa, respectively, as shown in Figures 1 and 2 as well as Figures S15 and S35. ScH_7 adopts the *Cmcm* structure ($Z = 4$, orthorhombic, Figure 7a) with eight quasi-
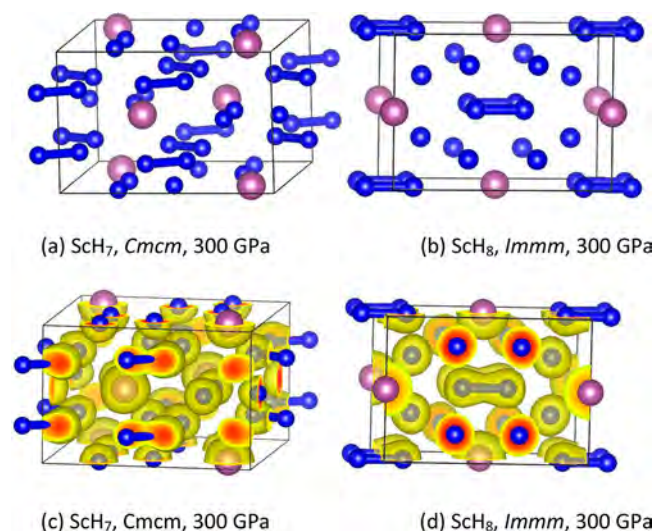
Figure 7. (a, b) Predicted ground-state static structures of (a) *Cmcm* ScH_7 and (b) *Immm* ScH_8 at 300 GPa. The lines indicate H−H separations shorter than 1.17 Å. Large balls are Sc, and small balls are hydrogen. (c, d) Three-dimensional ELF with isosurface values of 0.7.

molecular "H_2" units (H−H separations of 0.96 Å at 300 GPa) and 12 atomistic hydrogens in the unit cell of ScH_7 ($Sc_4(H_2)_8H_{12}$). The hydrogen atoms are in the same layer as the Sc atoms, while the "H_2" units form another layer. ScH_8 adopts an orthorhombic structure (*Immm*, $Z = 2$, Figure 7b). There are four quasi-molecular "H_2" units (H−H separations of 0.94 Å at 300 GPa) and eight atomistic hydrogens in the unit cell ($Sc_2(H_2)_4H_8$). In contrast to what we see in ScH_7, the "H_2" units are found in the same layer as the Sc atoms. The covalent interaction between two H atoms within the H_2 units is clearly visible from plots of the ELF, as shown in Figures 7c and 7d.

The interesting hydrogenic motifs of "H_5" pentagons or "H_8" octagons in ScH_9, ScH_{10}, and ScH_{12} are also clearly shown by the ELF calculated in specific planes of these hydrides, as shown in Figure 8. The ELF illustrates that ScH_{12} possesses a one-dimensional (1D) hydrogenic sublattice.

Still another way to visualize the geometries of these hydrogen-rich phases is via a polyhedral representation, the polyhedra marking the hydrogens close to a given Sc. There is a range of Sc−H separations in all structures, so one has to be careful to examine the distances to find a rational criterion for
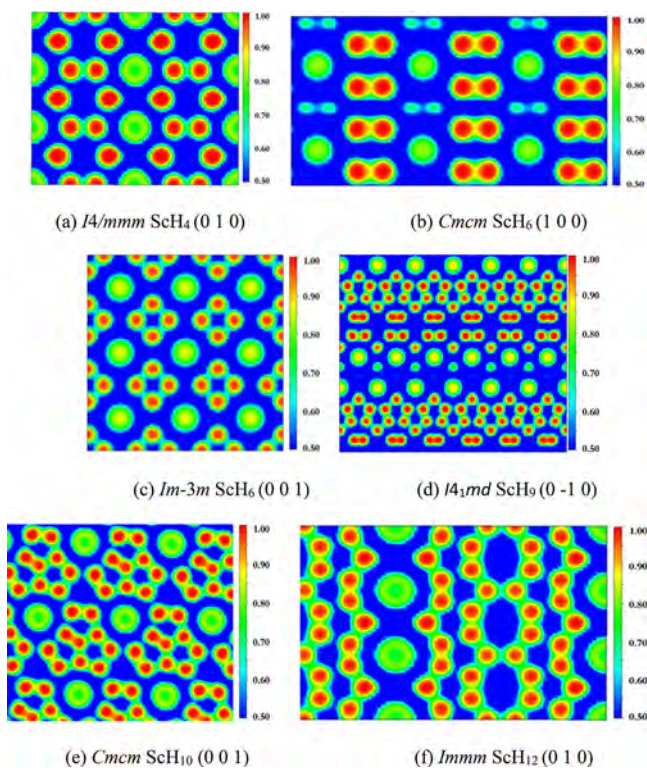
Figure 8. ELFs in the (a) (0 1 0) plane of $I4/mmm$ ScH_4 at 120 GPa, (b) (1 0 0) plane of $Cmcm$ ScH_6 at 200 GPa, (c) (0 0 1) plane of Im-$3m$ ScH_6 at 250 GPa, (d) (0 1 0) plane of $I4_1md$ ScH_9 at 300 GPa, (e) (0 0 1) plane of $Cmcm$ ScH_{10} at 250 GPa, and (f) (0 1 0) plane of $Immm$ ScH_{12} at 350 GPa. Large circles are Sc, and small circles are hydrogen.

drawing a polyhedron. Here histograms of Sc−H separations help. In Figure 9 we show these for some of the structures just discussed.
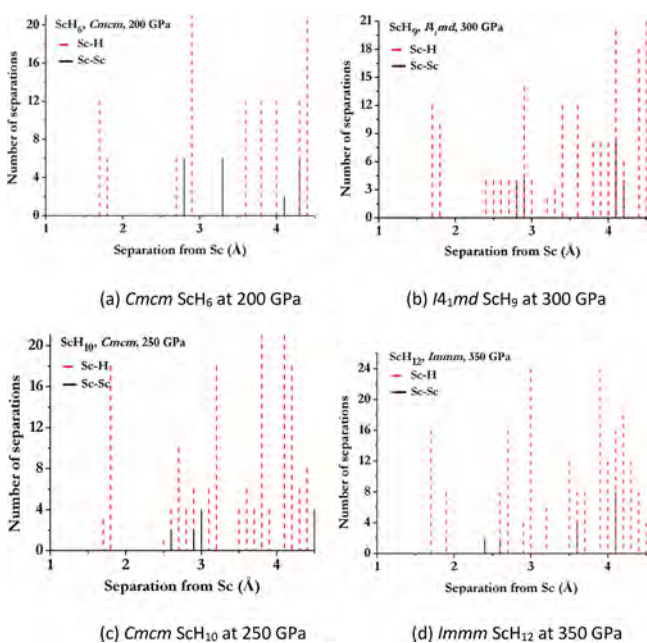
Figure 9. Histograms of Sc−H (red) and Sc−Sc (black) separations in (a) $Cmcm$ ScH_6 at 200 GPa, (b) $I4_1md$ ScH_9 at 300 GPa, (c) $Cmcm$ ScH_{10} at 250 GPa, and (d) $Immm$ ScH_{12} at 350 GPa.

The pressures are different for each structure in its stability range. This affects primarily the Sc−Sc separations. As for the Sc−H distances, note how there is a good window between separations around 1.7−1.8 Å (in ScH_2 and ScH_3 at 1 atm these are 1.76 and 1.82 Å, respectively) and the next Sc−H separation. This is our rationale for choosing 2.00 Å as the Sc−H cutoff distance. The polyhedra thus obtained are shown in Figure 10; they contain 18, 22, 21, and 24 hydrogens for
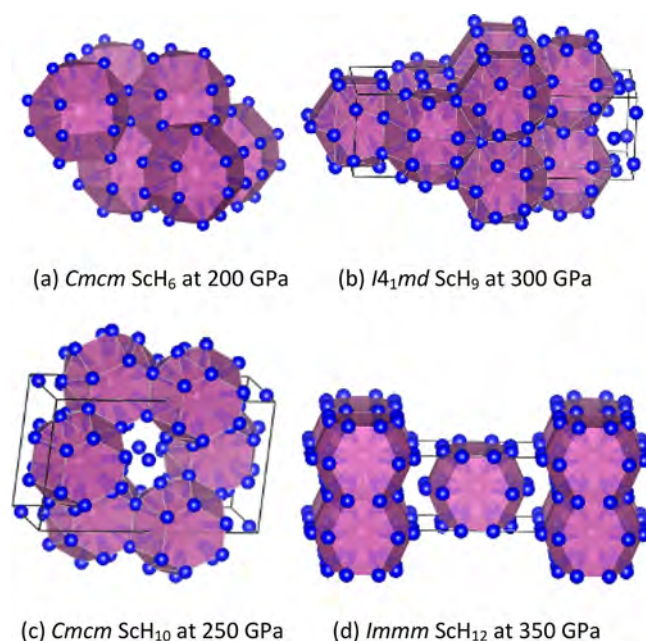
Figure 10. Polyhedra of hydrogens around each Sc atom in (a) $Cmcm$ ScH_6 at 200 GPa, (b) $I4_1md$ ScH_9 at 300 GPa, (c) $Cmcm$ ScH_{10} at 250 GPa, and (d) $Immm$ ScH_{12} at 350 GPa. Large balls are Sc, and small balls are hydrogen.

ScH_6, ScH_9, ScH_{10}, and ScH_{12}, respectively. The coordination number should increase with increasing number of hydrogen atoms and pressure, but "coordination" here is a complex descriptor, involving Sc−H, Sc−Sc, and H−H separations.

3.3. Interconversions of the Various Hydrides Incorporating the Effect of ZPE. As our discussion already showed, it is instructive to consider the stability regions of the higher scandium hydrides (and their transformations) in a language derived from the low hydrides—in terms of the incorporation of H_2 and its potential loss. If we do so, we find that many disproportionation and comproportionation reactions of the hydrides can occur. Indeed, the pressure-induced disproportionation of ScH_2 to ScH and ScH_3 was confirmed by both experimental[53] and theoretical results.[23] As we look at hydrogenation reactions among the higher hydrides, it becomes clear why zero point energies must be accounted for explicitly in the process, for molecular H_2 units have a high ZPE, the highest in the molecular realm.

The stability patterns with respect to H_2 addition and expulsion are shown for all stable stoichiometries in the Supporting Information. Here we only show the enthalpy curves probing decomposition and formation of ScH_6 and ScH_{12} with ZPE corrections. Figure 11 shows the enthalpy curves with respect to dissociation into ScH_3 or ScH_4 + solid H_2 of various structures of ScH_6. Unlike the convex hull diagram in Figure 1, figures similar to Figure 11 can tell us the
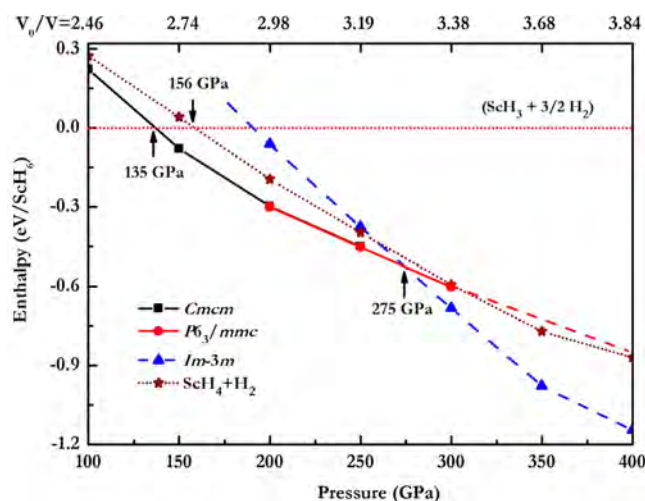
Figure 11. Enthalpy curves of various structures of ScH_6 relative to the products ScH_3 + solid H_2 as functions of pressure, ZPEs included. We have considered the most stable structures for ScH_3, ScH_4, and H_2 in their respective pressure ranges, as shown in Figure 2. The relative compression (V_0/V) is indicated.

exact pressures at which phase transitions occur, and figures such as these are required to construct Figure 2.

If we do this, we find (as mentioned earlier) that ScH_3 + solid H_2 will transform directly to ScH_6 ($Cmcm$, $Z = 4$,) above 135 GPa, rather than change to ScH_4 ($I4/mmm$, $Z = 2$) at 156 GPa. Going up in pressure, the $Cmcm$ structure of ScH_6 will then turn into a $P6_3/mmc$ ($Z = 2$) structure above 200 GPa. And above 275 GPa, the sodalite-like structure (Im-$3m$, $Z = 2$) of ScH_6 is preferred, as mentioned before. The transition pressures obtained from Figure 11 are in accordance with the convex hull diagram in Figure 1, where ScH_6 is the only stable hydride on the 150 GPa hull, and the global thermodynamic minimum on the 200 GPa hull. Figure 11 also tells us that the formation of ScH_6 from ScH_4 and H_2 is favorable in the stability range of these compounds. How do we reconcile this with the fact that ScH_6 goes off the hull at 300 and 350 GPa, only to return at 400 GPa? Figure 1 shows us that at these pressures the only points that lie on the hull whose enthalpies of formation are more negative than those of ScH_6 are ScH_4 and ScH_7. Indeed, as shown in Figure 12, where negative enthalpies mark a region of stability of ScH_6 and positive ones of ScH_4 + ScH_7, we find that the decomposition reaction $ScH_6 \rightarrow 2/3(ScH_7) + 1/3(ScH_4)$ is favorable in the narrow pressure range of 285−355 GPa.

Figure 13 provides the enthalpy curves of various structures of ScH_{12} relative to dissociation into ScH_3 + solid H_2 as a function of pressure, ZPE corrections included. The decomposition enthalpies for ScH_{12} with respect to ScH_n ($n = 4−11$) and molecular hydrogen are also presented. The convex hull diagram and Figure 13 predict that ScH_{12} will be stable above 325 GPa. We also find that the enthalpy of ScH_6 + $3H_2$ is higher than that of ScH_{10} + H_2 above 220 GPa. It suggests that the reaction of ScH_6 + $2H_2 \rightarrow ScH_{10}$ becomes enthalpically favorable at this pressure. Interestingly, above 285 GPa, the enthalpy of ScH_{10} + H_2 is higher than that of ScH_9 + $3/2H_2$. This suggests that the $Cmcm$ structure of ScH_{10} will decompose to the $I4_1md$ structure of ScH_9 and H_2. In general, phase separation reactions of hydrides are expected to be common under pressure, provided the kinetic barriers are not too high. Above 325 GPa, ScH_9 will continue to absorb hydrogen and
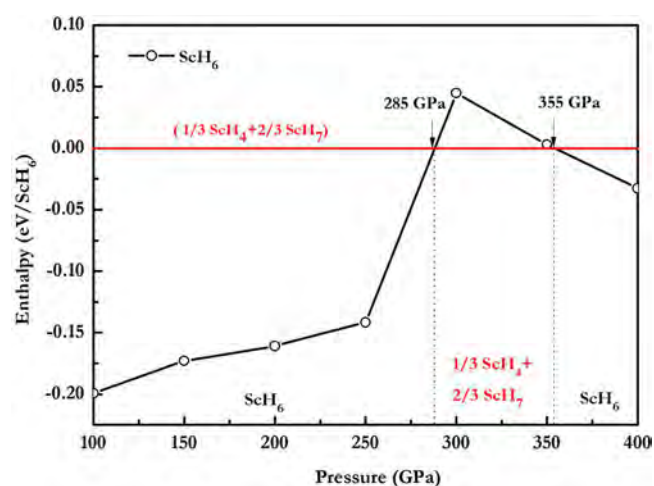
Figure 12. Enthalpy curves per formula unit of ScH_6 with respect to ScH_4 + ScH_7 including the ZPEs. We have considered the most stable structures for ScH_4, ScH_6, and ScH_7 found in this work at the specified pressure ranges.
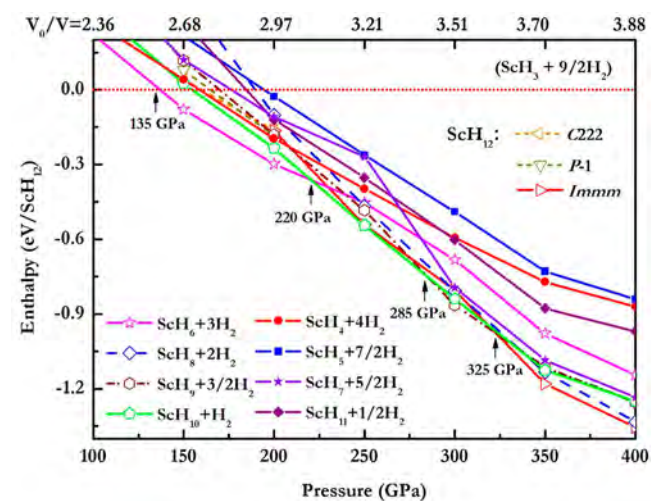
Figure 13. Enthalpy curves of various structures (P-1, $C222$, and $Immm$) of ScH_{12} relative to the products ScH_3 + solid H_2 as a function of pressure, ZPEs included. The decomposition enthalpies for ScH_{12} with respect to the most stable phases of ScH_n ($n = 4−11$) and molecular hydrogen are also provided. The relative compression (V_0/V) is indicated.

transform to the $Immm$ structure of ScH_{12}. Note that all the enthalpy curves in Figure 13 are close to each other; thus, our conclusions may be sensitive to the methodologies used, and the free energies associated with the reactions may be temperature-dependent.

We have now provided the justification for the phase stabilities summarized graphically in Figure 2. When the ZPEs are included, $I4/mmm$ ScH_4 is stabilized above 156 GPa, $Cmcm$ (or $P6_3/mmc$) ScH_6 from 135 to 275 GPa, Im-$3m$ ScH_6 between 275 and 285 GPa and then above 355 GPa, $Cmcm$ ScH_7 above 280 GPa, $Immm$ ScH_8 above 320 GPa, $I4_1md$ ScH_9 between 285 and 325 GPa, $Cmcm$ ScH_{10} between 220 and 285 GPa, and $Immm$ ScH_{12} above 325 GPa. In summary, considerations of ZPEs are important in determining which phases are stable and in finding the sequence of transformations that can occur between them. The stable phases found between 135 and 400 GPa in our study that have not been predicted

before include *Cmcm* ScH_6, *Cmcm* ScH_7, $I4_1md$ ScH_9, and *Immm* ScH_{12}. It is amazing that so many stable phases are found in the hydrides of scandium under pressure. The structures themselves contain fascinating hydrogenic arrangements, which we now explore.

3.4. Discussion. *Hydrogenic Motifs in ScH_n.* Hydrogen atoms/ions/molecules that are introduced into a Sc lattice must interact with or be bonded to the scandium ions. The geometry and strength (as gauged by the Sc−H separations) of these bonding interactions are of considerable interest, as is the effect of introduced hydrogen on the Sc−Sc bonding. Histograms of Sc−H, Sc−Sc, and H−H distances are shown in Figures S39−S46; some were shown earlier in Figure 9. In Figure 14 we show the shortest Sc−H and Sc−Sc separations in each phase at a single pressure point that lies in a region where the phase is (meta)stable.
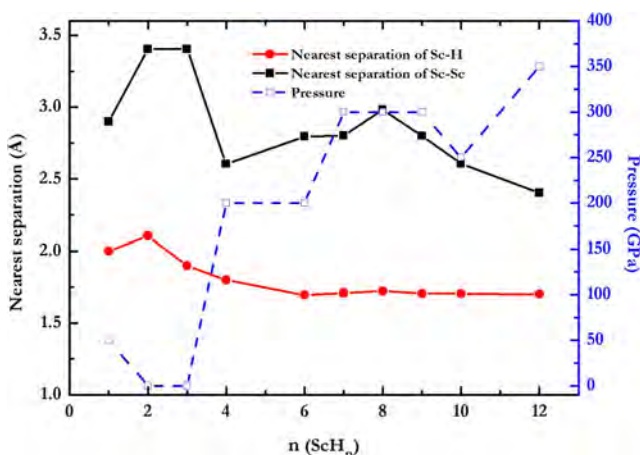
Figure 14. Nearest separations of Sc−H (red) and Sc−Sc (black) in ScH_n ($n = 1$−4, 6−10, 12) each at a single pressure point (blue hollow square). The pressure scale is on the right.

The shortest Sc−H separation changes from 2.07 Å ($n = 2$, 1 atm) to 1.70 Å ($n = 10$, 250 GPa) in ScH_n ($n = 1$−12), as n and pressure change. For a rough calibration, the calculated Sc−H separations in molecular hydrides ScH and ScH_2 at 1 atm are 1.76 and 1.82 Å, respectively.[54] As we noted above, it appears that Sc−H separations are not affected much by the hydrogen content of the associated scandium hydride, at least for static arrangements. The Sc−Sc separation varies more and generally decreases with pressure. The applied pressure and the extent of H introduction do not change the Sc−H separation in the lattice of scandium hydride a lot. This suggests that the admitted hydrogen atoms tend to interact with each other to form extended hydrogen motifs.

The shortest ground-state H−H separation is 1.19 Å in $I4/mmm$ ScH_4 at 200 GPa, 1.01 Å in *Cmcm* ScH_6 at 200 GPa, 0.85 Å in $I4_1md$ ScH_9 at 300 GPa, 0.85 Å in *Cmcm* ScH_{10} at 250 GPa, and 0.91 Å in *Immm* ScH_{12} at 350 GPa. These fall between the shortest inter- and intramolecular H−H distances in hydrogen itself at similar compression.[46] Several interesting types of hydrogenic species can be observed in higher hydrides of scandium, as noted earlier; they include monatomic H + molecular "H_2" (H−H separation 1.19 Å for ScH_4 at 200 GPa, 0.96 Å for ScH_7 at 300 GPa, and 0.94 Å for ScH_8 at 300 GPa) in ScH_4, ScH_7, and ScH_8, molecular "H_2" (H−H separation at 200 GPa, 1.10 Å) in ScH_6, molecular "H_2" + "H_5" pentagons (H−H separation at 300 GPa, 0.85−1.06 Å for "H_2" units,

1.01−1.17 Å for "H_5" units) in ScH_9, closed "H_5" pentagons edge-shared by two open "H_5" pentagons (H−H separation at 250 GPa, 0.86−1.10 Å for "H_5" units) in ScH_{10}, and an "H_8" octagon with six edges connected by "H_5" pentagons and the other two opposite edges connected by another "H_8" octagon (H−H separation at 350 GPa, 0.91−1.10 Å for "H_5" units and "H_8" units) in ScH_{12}. The latter case is shown in Figure 6. The interaction between H atoms is also clearly visible from the ELF plots; we have shown some of them in Figure 8.

H atoms form (closed or partially open) "H_5" pentagons or "H_8" octagons in ScH_9, ScH_{10}, and ScH_{12}. Such arrangements of hydrogen atoms have seldom been reported before.[5,6] In *Cmcm* ScH_{10} and *Immm* ScH_{12} one observes layered structures.

A Model for Explaining the H−H Distances in Scandium Hydrides. As suggested by Wang and co-workers,[4] the presence of different types of hydrogen motifs can be rationalized based on the effective number of electrons contributed by the Sc atom and accepted by hypothetical H_2 molecules in each stoichiometry. Assuming that the three valence electrons of each Sc atom are completely "ionized", moving off the metal atom to be accepted by H_2 molecules, the "formal" effectively added electron (EAE) count per H_2 for ScH_4 is $(3/2)e/H_2$, for ScH_6 it is $1e/H_2$, for ScH_9 it is $(2/3)e/H_2$, for ScH_{10} it is $(3/5)e/H_2$, and it is $(1/2)e/H_2$ for ScH_{12}. The transferred electrons must enter the H_2 antibonding σ_u^* orbitals, which consequently will weaken the H−H bond. Whether the H−H bond is subsequently stretched, or even dissociated, depends on the number of EAEs.[4,6]

The $I4/mmm$ structure of ScH_4 is the same as found for CaH_4,[4] SrH_4,[24,50] and also YH_4.[11] In ScH_4, there are three electrons available per two H_2 molecules. Therefore, one can imagine, formally, that one H_2 bond is completely broken into two monatomic hydrides, and the remaining one electron contributed by the Sc occupies the σ^*-orbital on the second H_2 at 200 GPa, thereby weakening the bond of that molecule and resulting in a longer H−H distance of 1.19 Å. Thus, the formula of the $I4/mmm$ ScH_4 phase can be written as $(Sc_2(H_2)_2(H)_4)$, containing two stretched molecular H_2 and four monatomic hydride units. In the case of ScH_6, one electron is formally added to each of the three H_2s. This is not enough to dissociate the H_2 molecule, and the H−H bond is elongated to 1.00 Å at 250 GPa. At this pressure ScH_6 has a hexagonal ($P6_3/mmc$, $Z = 2$) structure consisting entirely of molecular "H_2" units.

Extending this concept further, one would expect that ScH_9, ScH_{10}, and ScH_{12}, with a high H content (smaller EAE, less than one) would be composed predominantly of molecular hydrogen units with stretched H−H bonds. Actually, ScH_9 has a tetragonal ($I4_1md$, $Z = 4$) structure consisting of eight molecular and four "H_5" pentagonal hydrogen units $(Sc_4(H_2)_8[(H)_5]_4)$. There are 28 stretched H−H bonds in the unit cell of ScH_9, and each H−H bond accepts 0.43e on average based on the EAE. Thus, as this pressure, the model of "just" stretched, but still molecular H_2 units breaks down, and new aggregations of hydrogen, partially bonded to each other, evolve.

ScH_{10} has in our calculations an orthorhombic (*Cmcm*, $Z = 4$) structure consisting of four "H_{10}" units, each of which further consists of three edge-shared "H_5" pentagons (one closed "H_5" pentagon, the other two open). There are 40 stretched H−H bonds in the unit cell of ScH_{10}. Each H−H bond accepts on average 0.30e based on the EAE. Finally, ScH_{12} has an orthorhombic (*Immm*, $Z = 2$) structure consisting of two "H_{12}" units, each of which further consists of one "H_8" octagon edge-

shared by three "H$_5$" pentagons. There are 32 stretched H−H bonds in the unit cell of ScH$_{12}$. Each H−H bond has accepted 0.19e on average based on the EAE.

A Bader analysis (see Table S19) is overall not very informative. It does indicate (Table 1) the pretty much full ionic charge transfer between Sc and H atoms in the scandium hydrides.

Table 1. Bader Charges on the Hydrogen Atoms with the Shortest H−H Separation in the Scandium Hydrides

space group	pressure (GPa)	H−H distance (Å)	atom	δ (e)[a]
$Fm\text{-}3m$ ScH$_2$	1 atm	2.69	H	0.77
$I4/mmm$ ScH$_4$	120	1.18	H	0.22
$P6_3/mmc$ ScH$_6$	250	1.00	H	0.16
$I4_1md$ ScH$_9$	300	0.85	H	0.05
$Cmcm$ ScH$_{10}$	250	0.85	H	0.05
$Immm$ ScH$_{12}$	350	0.91	H	0.04
$I4/mmm$ YH$_4$	120	1.35	H	0.31

[a]δ is the charge accepted on average by each H atom with the shortest H−H separation.

Previous studies have shown that pressure-induced 4s−3d charge transfer turns Ca[4] or Sr[50] from an s-dominant metal into an s-d metal at high pressure, making these elements similar to Sc and Y.[11] Therefore, the presence of similar structure types in ScH$_4$, YH$_4$, CaH$_4$, and SrH$_4$ is not unexpected. However, the H−H distance in the "H$_2$" molecule in ScH$_4$ (1.18 Å) or (1.33 Å) in YH$_4$ is much longer than that (0.81 Å) in CaH$_4$ or (0.82 Å) in SrH$_4$ at 120 GPa, as Sc and Y transfer more valence electrons to H$_2$ than Ca or Sr. One would expect that Y will also transfer more electrons to H than Sc, since the electronegativity of Y (1.22) is less than that of Sc (1.36). This empirical consideration is supported by calculations of the Bader charges (see Table 1 and Table S19).

Electronic Structures of the Scandium Hydrides. The calculated electronic structures show that all of the higher hydrides of scandium under high pressure are metallic; their band structures are shown in the Supporting Information. Here we only show the electronic band structure and density of states (DOS) for the $Immm$ structure of ScH$_{12}$, a veritable spaghetti diagram (Figure 15). The significant overlap of Sc 3d states and the hydrogen 1s states suggests strong Sc−H interactions. By adding small amounts of scandium into hydrogen, we indeed obtain the metallization of hydrogen at a lower pressure. But further calculations, with functionals better suited for calculating reliable band gaps, are needed to see if the metallicity is retained.

The presence of the intriguing hydrogenic motifs gives rise to a relatively high DOS at E_F, such as 0.03 eV^{-1} per electron in $I4_1md$ ScH$_9$ at 300 GPa, 0.02 eV^{-1} per electron in $Cmcm$ ScH$_{10}$ at 250 GPa, and 0.03 eV^{-1} per electron in $Immm$ ScH$_{12}$ at 350 GPa. For comparison, the density of states at the Fermi level of $Im\bar{3}m$ CaH$_6$ (T_c = 235 K at 150 GPa),[4] $Im\bar{3}m$ YH$_6$ (T_c = 264 K at 120 GPa),[11] and $Im\bar{3}m$ ScH$_6$ all at 150 GPa are 0.02 eV^{-1} per electron, 0.04 eV^{-1} per electron, and 0.05 eV^{-1} per electron, respectively, as shown in the Supporting Information. The concurrence of flat and steep electronic bands near E_F (see Figure 15 and others in the Supporting Information) suggests a possibility of pairing of electrons at the Fermi level,[55] which is encouraging for superconductivity.

Superconducting Properties of the Scandium Hydrides. The hydrogenic motifs that have so far been theoretically
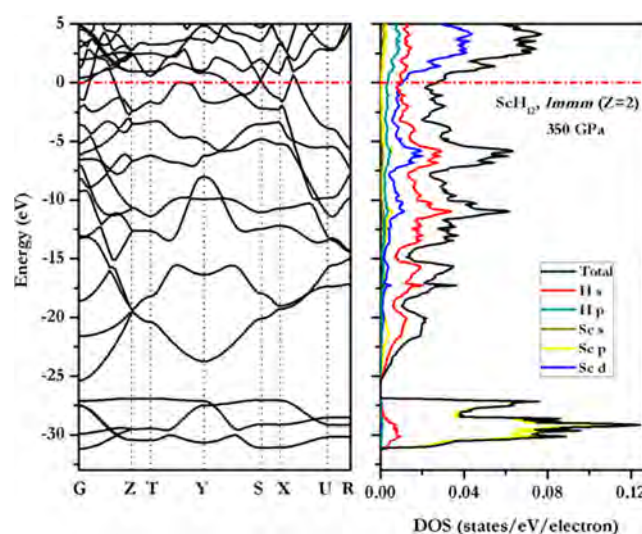
Figure 15. Electronic band structure and DOS for the $Immm$ structure of ScH$_{12}$ at 350 GPa.

predicted to constitute the high-pressure hydrides of the alkali and alkaline earth metals, as well as the group 3 elements Y and La, include H$^-$, H$_2^{\delta-}$, H$_2$, and H$_3^-$ units as well as the (charged) clathrate-like three-dimensional extended lattices present in CaH$_6$, MgH$_6$, YH$_6$, LaH$_{10}$, and the one-dimensional chains found in an $R\text{-}3m$ SrH$_6$ phase.[5,6,50] Molecular entities that are composed of stand-alone or fused hydrogenic polyhedral units, such as those found in ScH$_9$ or ScH$_{10}$, have not yet been observed. It has been noted that the high-pressure hydride phases with large predicted values of T_c typically possess a hydrogenic lattice that does not contain quasi-molecular H$_2$ or H$_3^-$ units[7] because the electronic structure of such systems is only weakly affected by the motion of the H atoms. The electron−phonon coupling (EPC) in phases with three-dimensional covalently bound networks containing hydrogen atoms (such as those found in H$_3$S or the aforementioned clathrate-like hydrogenic lattices), on the other hand, is strong. We therefore wondered how the hydrogenic motifs in ScH$_9$, ScH$_{10}$, and ScH$_{12}$ would influence the EPC and the predicted superconducting transition temperatures.

Toward this end, we calculated the phonon dispersions, phonon densities of states, Eliashberg spectral functions ($\alpha^2F(\omega)/\omega$), and the integrated EPC (λ) for a number of scandium polyhydride phases at pressures where they are dynamically stable. Figure 16 illustrates the results of our calculations for $Immm$ ScH$_{12}$ at 350 GPa. The corresponding results for ScH$_4$, ScH$_6$, ScH$_7$, ScH$_9$, and ScH$_{10}$ are presented in Figure S47.

The absence of any imaginary phonon modes confirms the dynamical stabilities of these compounds. As expected, the phonon spectra are separated into two frequency regions, with the low frequencies (<500 cm^{-1}) dominated by the vibrations of Sc atoms, while the high end of the spectrum features mainly H motions, as shown in Figure 16. In this system, the modes associated with the heavy and light atoms contribute 23% and 77% to the total λ, 1.23, respectively.

Most of the higher hydrides of scandium are found to be good superconductors with a high T_c as estimated by the modified McMillan formula, for example, 135 K for $Im\text{-}3m$ ScH$_6$ at 350 GPa, 169 K for $Cmcm$ ScH$_7$ at 300 GPa, 163 K for $I4_1md$ ScH$_9$ at 300 GPa, 120 K for $Cmcm$ ScH$_{10}$ at 250 GPa,
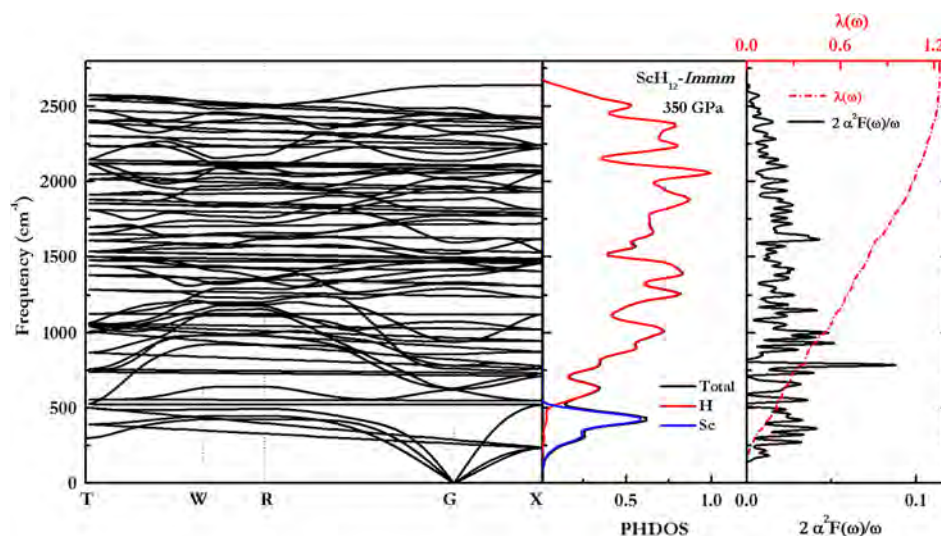
Figure 16. Phonon dispersion, projected phonon density of states (PHDOS), Eliashberg spectral function $\alpha^2F(\omega)/\omega$, and EPC coupling, $\lambda(\omega)$, of *Immm* ScH_{12} at 350 GPa.

and 141 K for *Immm* ScH_{12} at 350 GPa, as shown in Table 2. The average logarithmic frequencies (ω_{log}) of these species are

Table 2. Electron−Phonon Coupling Parameter (λ), Logarithmic Average Phonon Frequency (ω_{log}), and Computed Superconducting Transition Temperature (T_c) as Estimated via the Modified McMillan Equation (Estimates for the T_c Obtained via Numerically Solving the Eliashberg Equations Are Given in Parentheses) of Various Polyhydrides at Select Pressures for $\mu^* = 0.1$; Motifs Present in the Hydrogenic Lattices Are Also Provided

system	pressure (GPa)	λ	ω_{log} (K)	T_c (K)	hydrogenic motifs[a]
$P6/mmm$ ScH_2	300	0.44	543.5	4/−	H^-
$P6_3/mmc$ ScH_3	400	0.17	571.8	<1/−	H^-
$I4/mmm$ ScH_4	120	1.68	734.3	92 (163)	H^-, $H_2^{\delta-}$
$I4/mmm$ ScH_4	250	0.81	1891.8	68 (78)	H^-, $H_2^{\delta-}$
$P6_3/mmc$ ScH_6	250	0.57	1439.8	29 (43)	$H_2^{\delta-}$
$Im-3m$ ScH_6	350	1.25	1433.4	135 (169)	3-D
$Cmcm$ ScH_7	300	1.84	1245.2	169 (213)	H^-, $H_2^{\delta-}$
$I4_1md$ ScH_9	300	1.94	1156.2	163 (233)	$H_5^{\delta-}$ and $H_2^{\delta-}$
$Cmcm$ ScH_{10}	250	1.17	1366.8	120 (143)	$H_{10}^{\delta-b}$
$Immm$ ScH_{12}	350	1.23	1525.3	141 (194)	1-D

[a]For the purposes of clasifying the hydrogenic motifs that were present, we generally considered two hydrogens to be "bonded" if the ELF between them was at least 0.6. [b]Made from fused H_5 pentagons.

substantially larger than those of the scandium hydrides with "classic" stoichiometries (i.e., ScH_2 or ScH_3), which is a factor contributing to their larger T_c. However, a comparison of the T_c of the $P6_3/mmc$ and the $Im-3m$ phases of ScH_6, which have very similar ω_{log} values, reveals that the EPC parameter is the main factor responsible for a high superconducting critical temperature in these phases. The T_c of $I4/mmm$ ScH_4 is of the same magnitude as that predicted for YH_4 at 120 GPa, 84−95 K.[11,14] The T_c values as estimated via numerically solving the Eliashberg equations are larger than those computed with the modified McMillan equation, as expected. Interestingly, the systems with the largest EPC parameters ($I4/mmm$ ScH_4 at 120 GPa, $Cmcm$ ScH_7 at 300 GPa, and $I4_1md$ ScH_9 at 300 GPa)

contain $H_2^{\delta-}$ units. Phases with 1-D or 3-D hydrogenic lattices ($Im-3m$ ScH_6 and $Immm$ ScH_{12}) have the second largest set of λ values, followed by $Cmcm$ ScH_{10}, which contains the unique $H_{10}^{\delta-}$ molecular motifs. All other systems have an EPC parameter that is less than 1, with a concomitantly smaller T_c.

In the Supporting Information, we compare the superconducting properties of the scandium hydrides to the hydrides of Y and La, which are below Sc in the periodic table, and of Ca, which is to the left of Sc. There are many similarities in the high pressure chemistry of Y and La and a few for Ca.

4. CONCLUSIONS

We have explored structures of solid Sc−H systems at high pressures using the particle swarm optimization technique and evolutionary algorithms for structure searching. Some interesting structures of higher hydrides of scandium, ScH_4, ScH_6, ScH_7, ScH_8, ScH_9, ScH_{10}, and ScH_{12}, emerged as stable at pressures higher than 150 GPa. The intriguing interconversions between the various structures were studied. Unique hydrogenic motifs that have hitherto not been observed in other predicted high pressure hydrides, such as "H_5" pentagons or polyhedra formed from fused "H_5" pentagons and "H_8" octagons, are found in in ScH_9, ScH_{10}, and ScH_{12}. ScH_{10} and ScH_{12} adopt layered structures, and some very high coordination number polyhedra are found in the higher hydrides. For ScH_6, ScH_7, ScH_9, ScH_{10}, and ScH_{12} we predict high superconducting temperatures at high pressure, with the critical temperatures, as estimated via the modified McMillan equation, ranging from 120 to 169 K above 250 GPa (numerical solution of the Eliashberg equations yields T_c values between 143 and 233 K). We encourage experimentalists to attempt the synthesis of the higher hydrides, ScH_6, ScH_7, ScH_9, ScH_{10}, and ScH_{12}, by compressing mixtures of ScH_3 and H_2 above 150 GPa. The theoretical work carried out on the compressed polyhydrides to date suggests that systems with unusual stoichiometries containing Mg, Ca, Sc, Sr, Y, and La have the propensity for high-temperature superconductivity under pressure.

ASSOCIATED CONTENT

Ⓢ Supporting Information

The Supporting Information is available free of charge on the ACS Publications website at DOI: 10.1021/acs.jpcc.7b12124.

Structural parameters, enthalpies of select phases as a function of pressure, plots illustrating phase transitions, phonon band structures, density of states and electronic band structures, theoretical phase diagrams, histograms of Sc−H and Sc−Sc separations, Bader charges, Eliashberg spectral functions, detailed superconducting properties, and brief comparison of the hydrides of scandium with those of the neighboring elements (PDF)

AUTHOR INFORMATION

Corresponding Authors
*E-mail: ezurek@buffalo.edu (E.Z.).
*E-mail: rh34@cornell.edu (R.H.).

ORCID ⓘ
Eva Zurek: 0000-0003-0738-867X
Roald Hoffmann: 0000-0001-5369-6046

Notes
The authors declare no competing financial interest.

ACKNOWLEDGMENTS

REFERENCES

(1) Ashcroft, N. W. Hydrogen Dominant Metallic Alloys: High Temperature Superconductors? *Phys. Rev. Lett.* **2004**, *92*, 187002.

(2) Carlsson, A. E.; Ashcroft, N. W. Approaches for Reducing the Insulator-Metal Transition Pressure in Hydrogen. *Phys. Rev. Lett.* **1983**, *50*, 1305−1308.

(3) Zurek, E.; Hoffmann, R.; Ashcroft, N. W.; Oganov, A. R.; Lyakhov, A. O. A Little Bit of Lithium Does a Lot for Hydrogen. *Proc. Natl. Acad. Sci. U. S. A.* **2009**, *106*, 17640−17643.

(4) Wang, H.; Tse, J. S.; Tanaka, K.; Iitaka, T.; Ma, Y. Superconductive Sodalite-Like Clathrate Calcium Hydride at High Pressures. *Proc. Natl. Acad. Sci. U. S. A.* **2012**, *109*, 6463−6466.

(5) Zurek, E. Hydrides of the Alkali Metals and Alkaline Earth Metals under Pressure. *Comments Inorg. Chem.* **2017**, *37*, 78−98.

(6) Shamp, A.; Zurek, E. Superconductivity in Hydrides Doped with Main Group Elements under Pressure. *Novel Supercond. Mater.* **2017**, *3*, 14−22.

(7) Zhang, L.; Wang, Y.; Lv, J.; Ma, Y. Materials Discovery at High Pressures. *Nat. Mater. Rev.* **2017**, *2*, 17005.

(8) Gao, G.; Oganov, A. R.; Li, P.; Li, Z.; Wang, H.; Cui, T.; Ma, Y.; Bergara, A.; Lyakhov, A. O.; Iitaka, T.; Zou, G. High-Pressure Crystal Structures and Superconductivity of Stannane (SnH₄). *Proc. Natl. Acad. Sci. U. S. A.* **2010**, *107*, 1317−1320.

(9) Zaleski-Ejgierd, P.; Labet, V.; Strobel, T. A.; Hoffmann, R.; Ashcroft, N. W. WHₙ under Pressure. *J. Phys.: Condens. Matter* **2012**, *24*, 155701.

(10) Gao, G.; Hoffmann, R.; Ashcroft, N. W.; Liu, H.; Bergara, A.; Ma, Y. Theoretical Study of the Ground-State Structures and Properties of Niobium Hydrides under Pressure. *Phys. Rev. B: Condens. Matter Mater. Phys.* **2013**, *88*, 184104.

(11) Li, Y.; Hao, J.; Liu, H.; Tse, J. S.; Wang, Y.; Ma, Y. Pressure-Stabilized Superconductive Yttrium Hydrides. *Sci. Rep.* **2015**, *5*, 9948.

(12) Xie, Y.; Li, Q.; Oganov, A. R.; Wang, H. Superconductivity of Lithium-Doped Hydrogen under High Pressure. *Acta Crystallogr., Sect. C: Struct. Chem.* **2014**, *70*, 104−111.

(13) Feng, X.; Zhang, J.; Gao, G.; Liu, H.; Wang, H. Compressed Sodalite-Like MgH₆ as a Potential High-Temperature Superconductor. *RSC Adv.* **2015**, *5*, 59292−59296.

(14) Liu, H.; Naumov, I. I.; Hoffmann, R.; Ashcroft, N. W.; Hemley, R. J. Potential High-Tc Superconducting Lanthanum and Yttrium Hydrides at High Pressure. *Proc. Natl. Acad. Sci. U. S. A.* **2017**, *114*, 6990−6995.

(15) Drozdov, A. P.; Eremets, M. I.; Troyan, I. A.; Ksenofontov, V.; Shylin, S. I. Conventional Superconductivity at 203 K at High Pressures in the Sulfur Hydride System. *Nature* **2015**, *525*, 73−76.

(16) Duan, D.; Liu, Y.; Tian, F.; Li, D.; Huang, X.; Zhao, Z.; Yu, H.; Liu, B.; Tian, W.; Cui, T. Pressure-Induced Metallization of Dense (H₂S)₂H₂ with High-Tc Superconductivity. *Sci. Rep.* **2015**, *4*, 6968.

(17) Einaga, M. S.; Ishikawa, T.; Shimizu, K.; Eremets, M. I.; Drozdov, A. P.; Troyan, I. A.; Hirao, N.; Ohishi, Y. Crystal Structure of the Superconducting Phase of Sulfur Hydride. *Nat. Phys.* **2016**, *12*, 835−838.

(18) Drozdov, A. P.; Eremets, M. I.; Troyan, I. A. Superconductivity above 100 K in PH₃ at High Pressures. arXiv:1508.06224.

(19) Liu, H.; Li, Y.; Gao, G.; Tse, J. S.; Naumov, I. I. Crystal Structure and Superconductivity of PH₃ at High Pressures. *J. Phys. Chem. C* **2016**, *120*, 3458−3461.

(20) Shamp, A.; Terpstra, T.; Bi, T.; Falls, Z.; Avery, P.; Zurek, E. Decomposition Products of Phosphine under Pressure: PH₂ Stable and Superconducting? *J. Am. Chem. Soc.* **2016**, *138*, 1884−1892.

(21) Flores-Livas, J. A.; Amsler, M.; Heil, C.; Sanna, A.; Boeri, L.; Profeta, G.; Wolverton, C.; Goedecker, S.; Gross, E. K. U. Superconductivity in Metastable Phases of Phosphorus-Hydride Compounds under High Pressure. *Phys. Rev. B: Condens. Matter Mater. Phys.* **2016**, *93*, 020508.

(22) Ye, X.; Tang, T.; Ao, B.; Luo, D.; Sang, G.; Zhu, H. Thermodynamics of Sc-H and Sc-D Systems: Experimental and Theoretical Studies. *J. Fusion Energy* **2013**, *32*, 254−257.

(23) Ye, X.; Hoffmann, R.; Ashcroft, N. W. Theoretical Study of Phase Separation of Scandium Hydrides under High Pressure. *J. Phys. Chem. C* **2015**, *119*, 5614−5625.

(24) Hooper, J.; Terpstra, T.; Shamp, A.; Zurek, E. Composition and Constitution of Compressed Strontium Polyhydrides. *J. Phys. Chem. C* **2014**, *118*, 6433−6447.

(25) Wei, Y.; Yuan, J.; Khan, F. I.; Ji, G. F.; Gu, Z. W.; Wei, D. Q. Pressure Induced Superconductivity and Electronic Structure Properties of Scandium Hydrides using First Principles Calculations. *RSC Adv.* **2016**, *6*, 81534−81541.

(26) Kim, D. Y.; Scheicher, R. H.; Mao, H. K.; Kang, T. W.; Ahuja, R. General Trend for Pressurized Superconducting Hydrogen-Dense Materials. *Proc. Natl. Acad. Sci. U. S. A.* **2010**, *107*, 2793−2796.

(27) Abe, K. Hydrogen-Rich Scandium Compounds at High Pressures. *Phys. Rev. B: Condens. Matter Mater. Phys.* **2017**, *96*, 144108.

(28) Qian, S.; Sheng, X.; Yan, X.; Chen, Y.; Song, B. Theoretical Study of Stability and Superconductivity of ScHₙ(n = 4−8) at High Pressure. *Phys. Rev. B: Condens. Matter Mater. Phys.* **2017**, *96*, 094513.

(29) Peng, F.; Sun, Y.; Pickard, C. J.; Needs, R. J.; Wu, Q.; Ma, Y. Hydrogen Clathrate Structures in Rare Earth Hydrides at High Pressures: Possible Route to Room-Temperature Superconductivity. *Phys. Rev. Lett.* **2017**, *119*, 107001.

(30) Wang, Y.; Lv, J.; Zhu, L.; Ma, Y. Crystal Structure Prediction via Particle-Swarm Optimization. *Phys. Rev. B: Condens. Matter Mater. Phys.* **2010**, *82*, 094116.

(31) Lonie, D. C.; Zurek, E. XtalOpt: An Open-Source Evolutionary Algorithm for Crystal Structure Prediction. *Comput. Phys. Commun.* **2011**, *182*, 372−387.

(32) Kruglov, I. A.; Kvashnin, A. G.; Goncharov, A. F.; Oganov, A. R.; Lobanov, S.; Holtgrewe, N.; Yanilkin, A. Y. High-Temperature Superconductivity of Uranium Hydrides at Near-Ambient Conditions. 2017; https://arxiv.org/abs/1708.05251.

(33) Perdew, J. P.; Burke, K.; Ernzerhof, M. Generalized Gradient Approximation Made Simple. *Phys. Rev. Lett.* **1996**, *77*, 3865−3868.

(34) Kresse, G.; Furthmüller, J. Furthmüller. Efficient Iterative Schemes for Ab Initio Total-Energy Calculations using a Plane-Wave Basis Set. *Phys. Rev. B: Condens. Matter Mater. Phys.* **1996**, *54*, 11169−11186.

(35) Blöchl, P. E. Projector Augmented-Wave Method. *Phys. Rev. B: Condens. Matter Mater. Phys.* **1994**, *50*, 17953−17979.

(36) Monkhorst, H. J.; Pack, J. D. Special Points for Brillouin-Zone Integrations. *Phys. Rev. B* **1976**, *13*, 5188−5192.

(37) Togo, A.; Oba, F.; Tanaka, I. First-principles Calculations of the Ferroelastic Transition Between Rutile-Type and $CaCl_2$-type SiO_2 at High Pressures. *Phys. Rev. B: Condens. Matter Mater. Phys.* **2008**, *78*, 134106.

(38) Giannozzi, P.; Baroni, S.; Bonini, N.; Calandra, M.; Car, R.; Cavazzoni, C.; Ceresoli, D.; Chiarotti, G. L.; Cococcioni, M.; Dabo, I.; et al. QUANTUM ESPRESSO: a Modular and Open-Source Software Project for Quantum Simulations of Materials. *J. Phys.: Condens. Matter* **2009**, *21*, 395502.

(39) Troullier, N.; Martins, J. L. Efficient Pseudopotentials for Plane-Wave Calculations. *Phys. Rev. B: Condens. Matter Mater. Phys.* **1991**, *43*, 1993−2006.

(40) Garrity, K. F.; Bennett, J. W.; Rabe, K. M.; Vanderbilt, D. Pseudopotentials for High-Throughput DFT Calculations. *Comput. Mater. Sci.* **2014**, *81*, 446−452.

(41) http://physics.rutgers.edu/gbrv (accessed Jan 2018).

(42) Methfessel, M.; Paxton, A. T. High-Precision Sampling for Brillouin-Zone Integration in Metals. *Phys. Rev. B: Condens. Matter Mater. Phys.* **1989**, *40*, 3616−3621.

(43) Gonze, X.; Lee, C. Dynamical Matrices, Born Effective Charges, Dielectric Permittivity Tensors, and Interatomic Force Constants from Density-Functional Perturbation Theory. *Phys. Rev. B: Condens. Matter Mater. Phys.* **1997**, *55*, 10355−10368.

(44) Allen, P. B.; Dynes, R. C. Transition Temperature of Strong-Coupled Superconductors Reanalyzed. *Phys. Rev. B* **1975**, *12*, 905−922.

(45) Eliashberg, G. M. Interactions between Electrons and Lattice Vibrations in a Superconductor. *Sov. Phys. JETP* **1960**, *11*, 696−976.

(46) Labet, V.; Hoffmann, R.; Ashcroft, N. W. A Fresh Look at Dense Hydrogen under Pressure. III. Two Competing Effects and the Resulting Intra-Molecular H-H Separation in Solid Hydrogen under Pressure. *J. Chem. Phys.* **2012**, *136*, 074503.

(47) Akahama, Y.; Fujihisa, H.; Kawamura, H. New Helical Chain Structure for Scandium at 240 GPa. *Phys. Rev. Lett.* **2005**, *94*, 195503.

(48) Lityagina, L. M.; Dyuzheva, T. I. Isothermal Compression Study of 3d and 4d Transition Metal Dihydrides I: Compression of ScH_2 up to 27 GPa. *J. Alloys Compd.* **1992**, *179*, 69−71.

(49) Savin, A.; Nesper, R.; Wengert, S.; Fässler, T. F. The Electron Localization Function. *Angew. Chem., Int. Ed. Engl.* **1997**, *36*, 1808−1832.

(50) Wang, Y.; Wang, H.; Tse, J. S.; Iitaka, T.; Ma, Y. Structural Morphologies of High-Pressure Polymorphs of Strontium Hydrides. *Phys. Chem. Chem. Phys.* **2015**, *17*, 19379−19385.

(51) Segall, M. D.; Lindan, P. J. D.; Probert, M. J.; Pickard, M. J.; Hasnip, P. J.; Clark, S. J.; Payne, M. C. First-Principles Simulation: Ideas, Illustrations and the CASTEP code. *J. Phys.: Condens. Matter* **2002**, *14*, 2717−2744.

(52) Pickard, C. J.; Martinez-Canales, M.; Needs, R. J. Density Functional Theory Study of Phase IV of Solid Hydrogen. *Phys. Rev. B: Condens. Matter Mater. Phys.* **2012**, *85*, 214114.

(53) Machida, A.; Honda, M.; Hattori, T.; Sano-Furukawa, A.; Watanuki, T.; Katayama, Y.; Aoki, K.; Komatsu, K.; Arima, H.; Ohshita, H.; et al. Formation of NaCl-Type Monodeuteride LaD by the Disproportionation Reaction of LaD_2. *Phys. Rev. Lett.* **2012**, *108*, 205501.

(54) Wang, X.; Chertihin, G. V.; Andrews, L. Matrix Infrared Spectra and DFT Calculations of the Reactive MH_x (x = 1, 2, and 3), $(H_2)MH_2$, MH_2^+, and $MH_4^−$ (M = Sc, Y, and La) Species. *J. Phys. Chem. A* **2002**, *106*, 9213−9225.

(55) Simon, A. Superconductivity and Chemistry. *Angew. Chem., Int. Ed. Engl.* **1997**, *36*, 1788−1806.